AGU PUBLICATIONS

Geophysical Research Letters

RESEARCH LETTER
10.1002/2015GL064721

Key Points:
- *T* phase can be observed in global seismogram stacks
- *T* phase can be observed at stations up to 4° degrees inland from the coast
- Our results agree with the theory of acoustic to seismic coupling of the energy at continents

Correspondence to:
J. S. Buehler,
jsbuehle@ucsd.edu

Citation:
Buehler, J. S., and P. M. Shearer (2015), *T* phase observations in global seismogram stacks, *Geophys. Res. Lett.*, *42*, 6607–6613, doi:10.1002/2015GL064721.

Received 27 MAY 2015
Accepted 16 JUL 2015
Accepted article online 20 JUL 2015
Published online 18 AUG 2015

T phase observations in global seismogram stacks

J. S. Buehler[1] and P. M. Shearer[1]

[1]Scripps Institution of Oceanography, University of California, San Diego, California, USA

Abstract The *T* phase, conversion of acoustic to seismic energy, is typically observed as a high-frequency wave train at hydrophones or coastal seismic stations. Here we show that the *T* phase can be observed in broadband waveform stacks of ~5200 earthquakes recorded by the Global Seismic Network. To enhance the phase arrivals in stacks, we apply short-time window average over long-time window average filtering to individual traces before stacking. Although the *T* phase arrival is visible in stacks from seismograms filtered at 0.5–5 Hz, it appears much stronger at higher frequencies (2–8 Hz) and is further enhanced by only stacking seismograms from oceanic paths. Stacking only subsets of the data depending on continental path lengths on the receiver side shows that the *T* phase can be observed at stations up to 4° inland from the coast, and changes in the *T* phase arrival time correspond to reasonable crustal velocities.

1. Introduction

When seismic energy radiated from earthquakes below the ocean floor enters the water, it can generate an acoustic wave called the *T* phase. After traveling through the SOFAR channel, the sound waves may convert to crustal seismic waves when they encounter a continental slope [e.g., *Talandier and Okal*, 1998; *Okal*, 2008]. These arrivals can be observed in seismograms from receivers on land. Although most often recognized at coastal stations (or hydrophones), *T* phases can have large continental paths on the receiver end and have been observed at land stations several hundred kilometers away from the coast [*Cansi and Bethoux*, 1985; *Stevens et al.*, 2001]. The *T* phase is observed late in the seismogram, after the *P* and *S* arrivals, as they travel with lower speed through the ocean as part of their path. They are typically observed as higher frequency arrivals with a characteristically long wave train [*de Groot-Hedlin and Orcutt*, 1999]. The apparent propagation velocity will vary depending on the length of the continental portion of the path, but we expect it to be close to 1.5 km/s, the speed of sound in the ocean.

The conversion from acoustic to seismic energy at the continental slope is complex and not well understood [*Stevens et al.*, 2001; *Talandier and Okal*, 1998]. It has been observed that the attenuation of *T* phases along continental or island paths can be high [*Walker et al.*, 1992a; *Rodgers and Harben*, 2000]. Stacking of waveforms can often enhance such weak arrivals. Here we follow a previous stacking approach of *Astiz et al.* [1996] but with a more extensive global data set. We show that a clear *T* phase signal can be observed in broadband seismogram stacks from data from the Global Seismic Network (GSN), and demonstrate the change in apparent velocity of the signal with path length on land.

2. Data Selection and Stacking Procedure

For our seismology research program, we generated a database of broadband data from the GSN for ~5200 $M \geq 5.7$ events between 1988 and 2014. For each event, we saved 61 min of data from all the GSN stations, starting 1 min before the origin time (in retrospect, for *T* phase analysis it would have been better to save a longer time window, as our stacking results suggest *T* phase visibility beyond our 1 h window). Using this database, we then applied the seismogram stacking approach of *Astiz et al.* [1996]. The seismograms are mostly sampled at 20 Hz, and for simplicity we disregard any seismogram sampled at a different rate. We demean and filter the vertical component seismograms, compute the ratio function from a short-time window average (STA) and a long-time window average (LTA) for each trace [*Earle and Shearer*, 1994] and stack the STA/LTA functions within uniformly spaced time and distance bins. Figure 1 shows the 5200 source and 430 receiver locations for the ~531,000 seismograms used for our stacks.

Both stacking and STA/LTA filtering, which acts as a type of automatic gain control, can enhance weak arrivals [e.g., *Richards-Dinger and Shearer*, 1997; *Buehler and Shearer*, 2013]. Our initial stacks used a short-time window

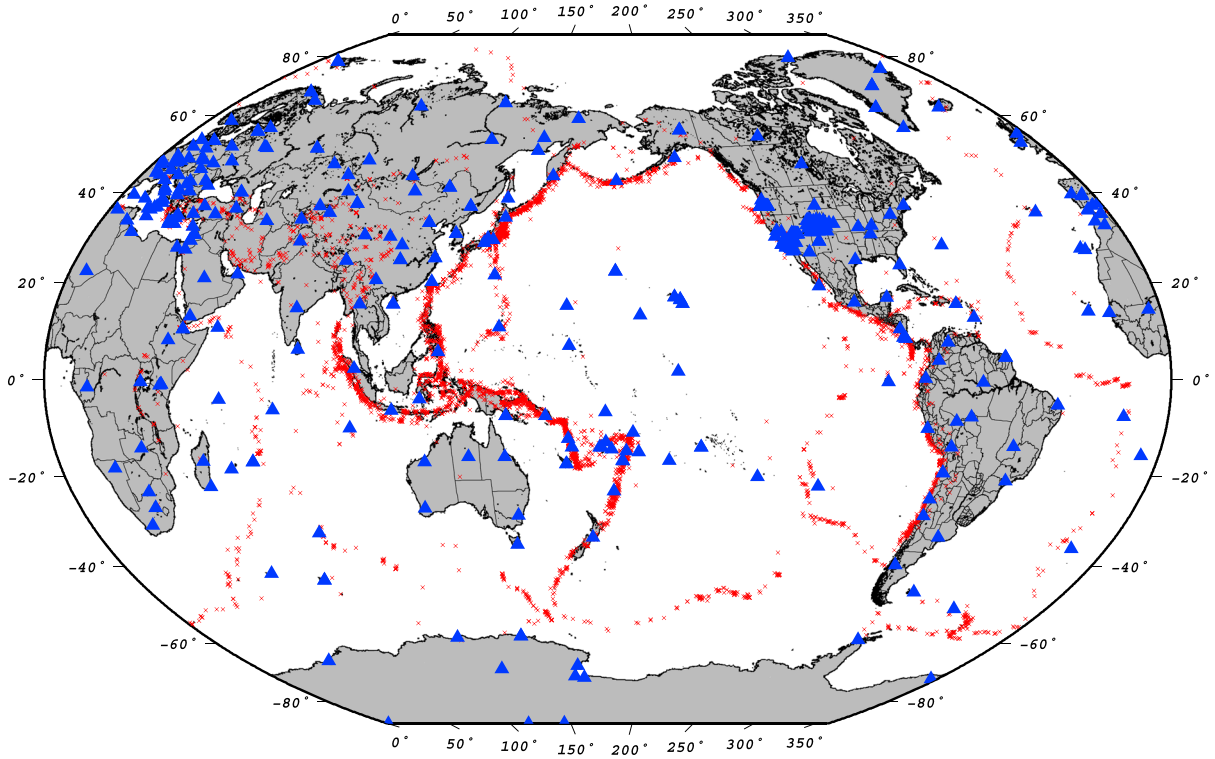

Figure 1. Receivers (blue triangles) and sources (red crosses) for the seismograms used in the stacks.

of 1 s and a long-time window of 10 s to produce global waveform stacks. Later we also applied a longer LTA window of 30 to 60 s to further enhance the *T* phase, especially when only using subsets of data. Because the *T* phase often is characterized by a long wave train, a short LTA window may decrease the ratio function before the highest amplitude part of the *T* phase arrival. We then stack the traces in time and distance bins of 2 s and 0.5°, respectively, and normalize them by the number of data points per bin. We limit the event depth to 50 km to avoid depth phases and time misalignment from the earlier arrivals produced by deeper events. The quality control we apply is very minimal, and we simply disregard any trace with a maximum STA/LTA value lower than 2.5. In addition, to avoid spikes and streaks in the image and to limit the influence of any single trace, we saturate the STA/LTA values at 10.

Following our global stacks of all the data, we compute separate stacks for terrestrial and oceanic paths. We trace great-circle paths between source and receiver, and for each path we find the distance it travels across land and ocean, respectively. We then compute stacks for various land/ocean percentages, and also fixed degrees, of the land portion on the receiver end of the path. This approach allows us to confirm if the changes of the *T* phase character in the stacks correspond with realistic crustal seismic velocities.

3. *T* Phase Observations

Figure 2a shows the broadband stack for the vertical component from seismograms filtered between 0.5 and 5 Hz from ~531,000 traces. The first *P* arrival appears strongest, followed by its multiples and the *S* wave arrivals. In addition, we observe a very late and weak feature in this image. The apparent velocity of this arrival falls between 1.45 and 1.6 km/s, strongly suggesting this is the *T* phase recorded at land seismometers of the GSN. Further, the feature becomes more visible in an image constructed with higher-frequency filtered seismograms (2–8 Hz, Figure 2b), appears even more strongly if we only stack seismograms from paths that are at least 80% oceanic (Figure 2c), and disappears if only the land paths are stacked (Figure 2d). In the oceanic path image (Figure 2c), the *T* phase is visible to ~50° and likely would be visible at longer ranges if it were not truncated by the 1 h limit of our database.

Figure 3 shows examples of seismograms in record section format for two different earthquakes. Observations show a clear signal in the *T* phase window for paths that traveled mostly across the ocean (blue traces

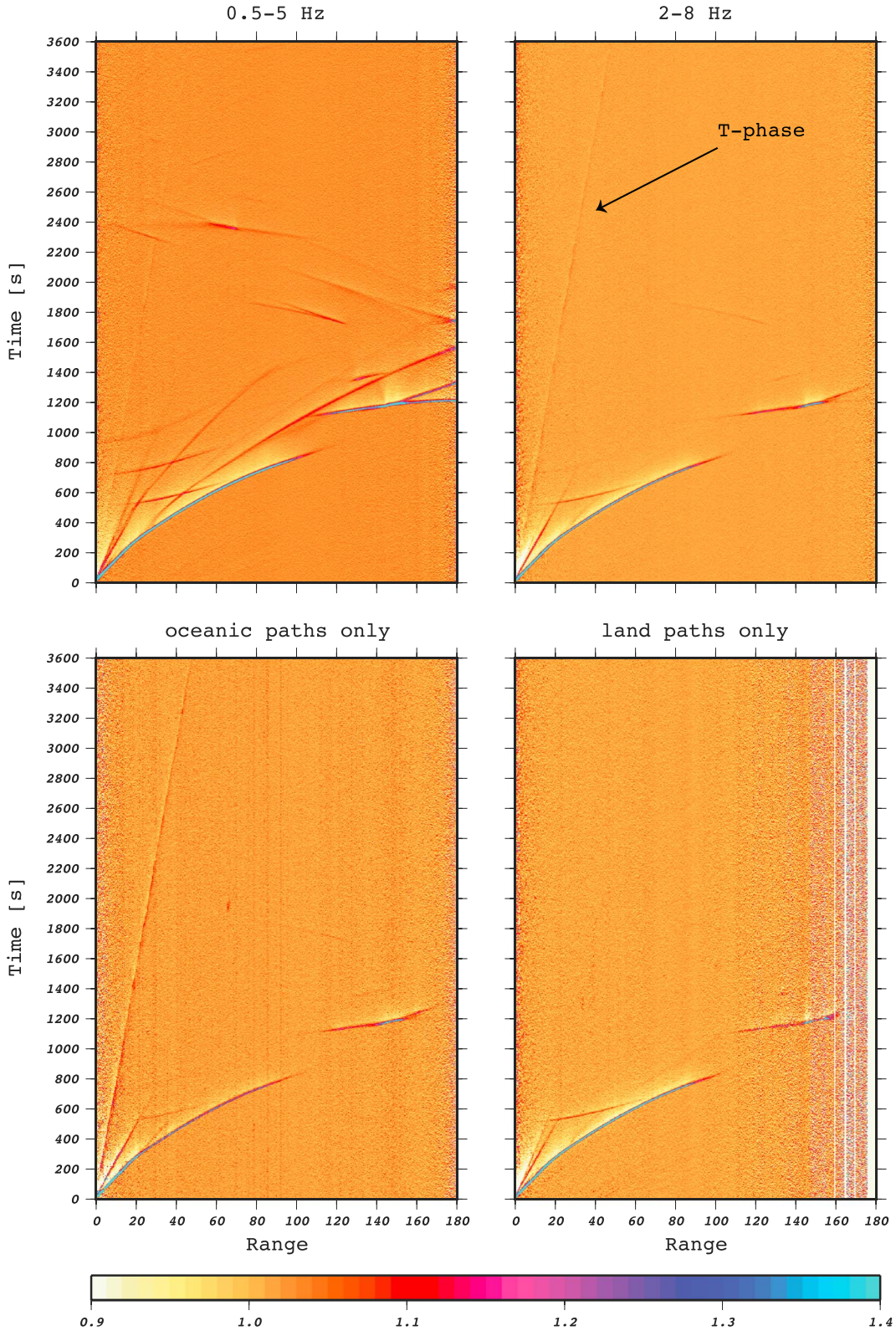

Figure 2. Global broadband STA/LTA seismogram stack. (a) Seismograms filtered between 0.5 and 5 Hz before stacking. A faint feature with apparent velocity of 1.5 km/s is visible. (b) Stack with traces filtered at 2–8 Hz. (c) Stack with oceanic paths only. (d) Stack with land paths only.

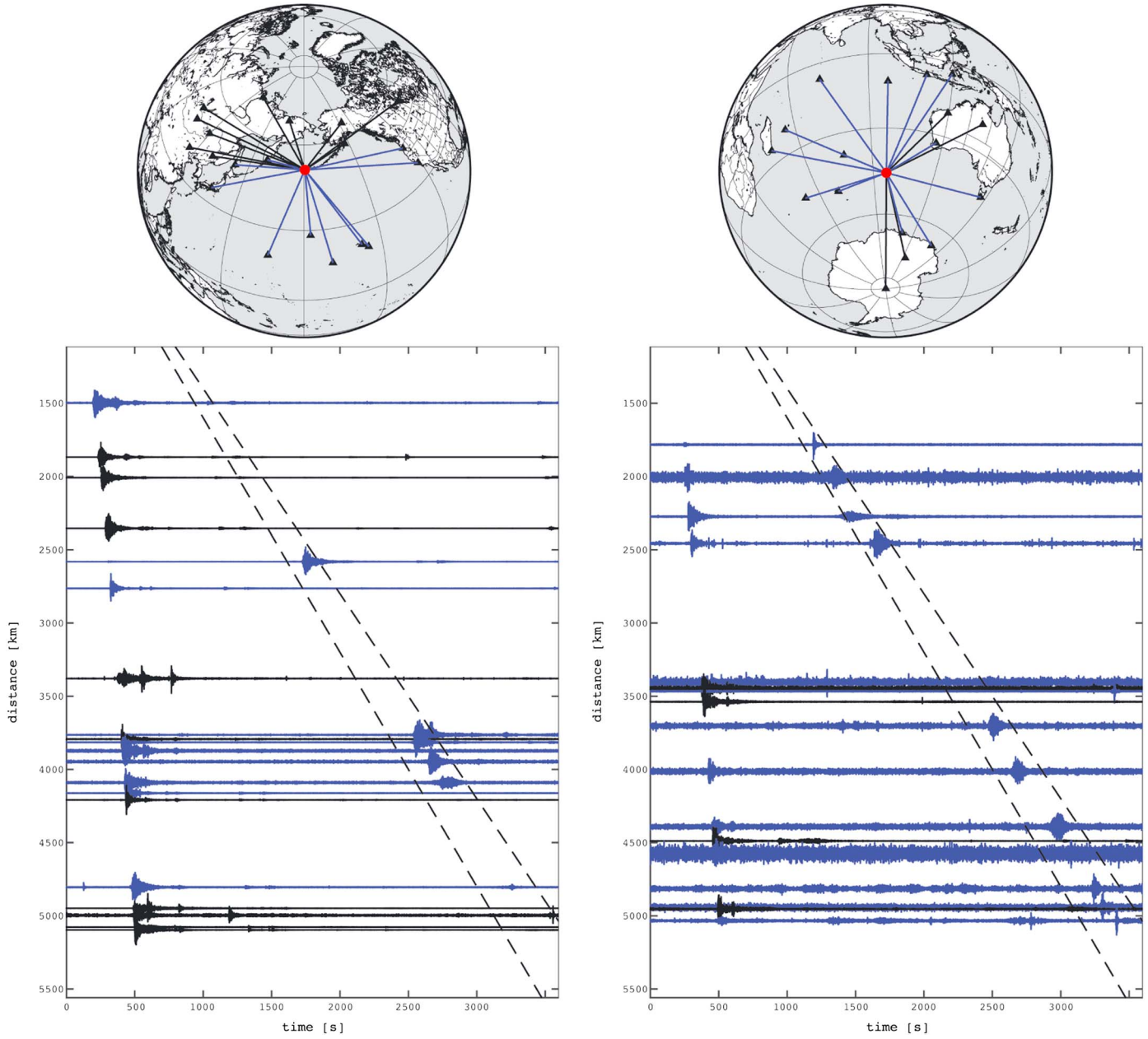

Figure 3. Example record sections. Seismograms from oceanic paths are plotted in blue, continental paths in black. Black dotted lines indicate arrival times for an apparent velocity between 1.4 and 1.6 km/s.

and blue paths on map). In contrast, records from continental paths (black traces and black paths on map) do not have clear T-phase arrivals. The signature of the observed *T* phase varies among the different stations, but the energy of the wave train generally ramps up slowly. It is not surprising that T-phases are not observed equally strong everywhere and that their character shows large variations, as bathymetry, continental slope, and sediment cover influence *T* phase propagation and energy transfer [e.g., *de Groot-Hedlin and Orcutt*, 1999, 2001].

Our stacks combine data from thousands of different ray paths. To identify the paths that contribute most to the *T* phase image, we search for paths that have STA/LTA values within the *T* phase window above a certain threshold (we consider a STA/LTA value of 2.5 as a good signal-to-noise ratio). Since this yields too many paths to plot them individually, we then proceed as follows: We divide the Earth's surface into 10 by 10° cells. We compute the mean amplitudes of the STA/LTA traces both in a 2 min window around the *T* phase and a control

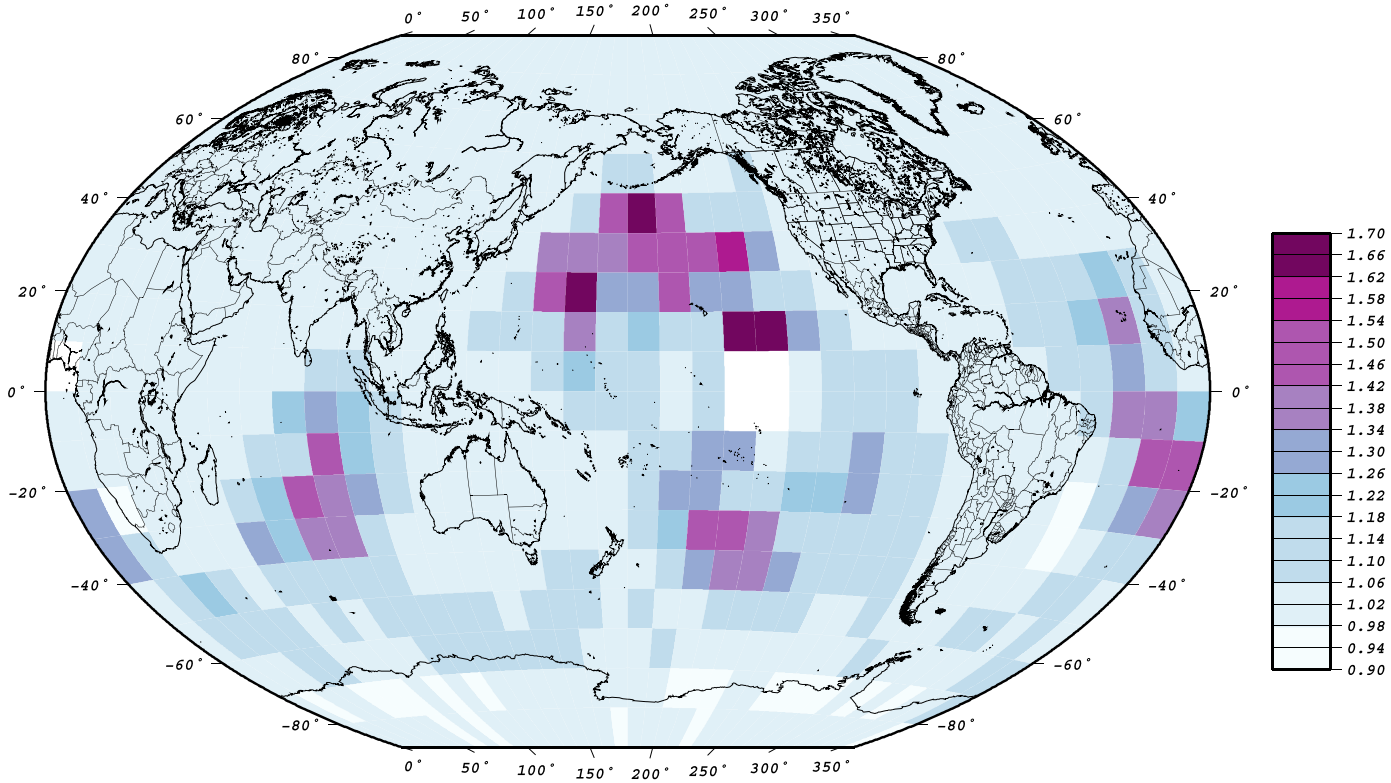

Figure 4. Mean signal-to-noise value in each 10° grid cell for all crossing traces. Signal to noise is computed as the mean amplitudes of the STA/LTA traces both in a 2 min window around the *T* phase and a control window of equal length immediately following the theoretical *T* phase. As expected, most large amplitudes in the *T* phase window are observed for oceanic paths. White cells do not have amplitude measurements (the white patch in the pacific is caused by the 1 h cut off of the seismograms, limiting the *T* phase observations to less than 50 degree range.

window of equal length immediately following the theoretical *T* phase time for all the seismograms that contribute to the stack and define the signal to noise as the ratio of these two amplitudes. For each grid cell, we find the crossing paths and the corresponding signal-to-noise values of these traces. Figure 4 shows the ratio of the mean signal to noise at each location for seismograms filtered at 2 to 8 Hz. It shows clearly that mostly oceanic paths have large amplitudes in the *T* phase windows. It would be interesting to further analyze where the *T* phase propagates efficiently and where it is attenuated or blocked. However, since the *T* phase character in individual seismograms shows large variations, and the STA/LTA parameters are kept fixed in the stacks, imaging the propagation efficiency by measuring the amplitudes in STA/LTA stacks is not straightforward.

However, similar stacking approaches to those shown here could be used in more detailed studies of *T* phase propagation processes. For example, it might be possible to study directionality and propagation efficiency of the *T* phase by stacking various subsets of source and receiver combinations for different frequency bands. This should help to improve our knowledge of both the seismic-to-acoustic and acoustic-to-seismic energy conversion systems and our understanding of the influence of topographic features on both the excitation and propagation processes [*Johnson et al.*, 1963; *Walker et al.*, 1992b; *Chapman and Marrett*, 2006]. In addition, globally imaged areas of increased *T* phase transmission could identify spatial and temporal variations of SOFAR channel properties. Future studies should examine much longer time windows than 1 h (which limits our *T* phase results to source-receiver distances of less than 50°) to allow more complete ray coverage across the Pacific. Finally, it will be important to assess whether *T* phases are only visible along certain paths after stacking data to enhance the signal to noise in weak arrivals or whether they are always seen on at least some individual seismograms. In the latter case, there will be a greater opportunity to study *T* phase amplitude variability and relate it to fine-scale details in the propagation paths. In any case, our stacking approach can provide a guide to where *T* phases are most readily observable for follow-up studies.

The apparent velocity of the *T* phase should change depending on the continental path length. We ran several stacks restricting the continental path lengths to a percentage of the total path length as well as to a fixed

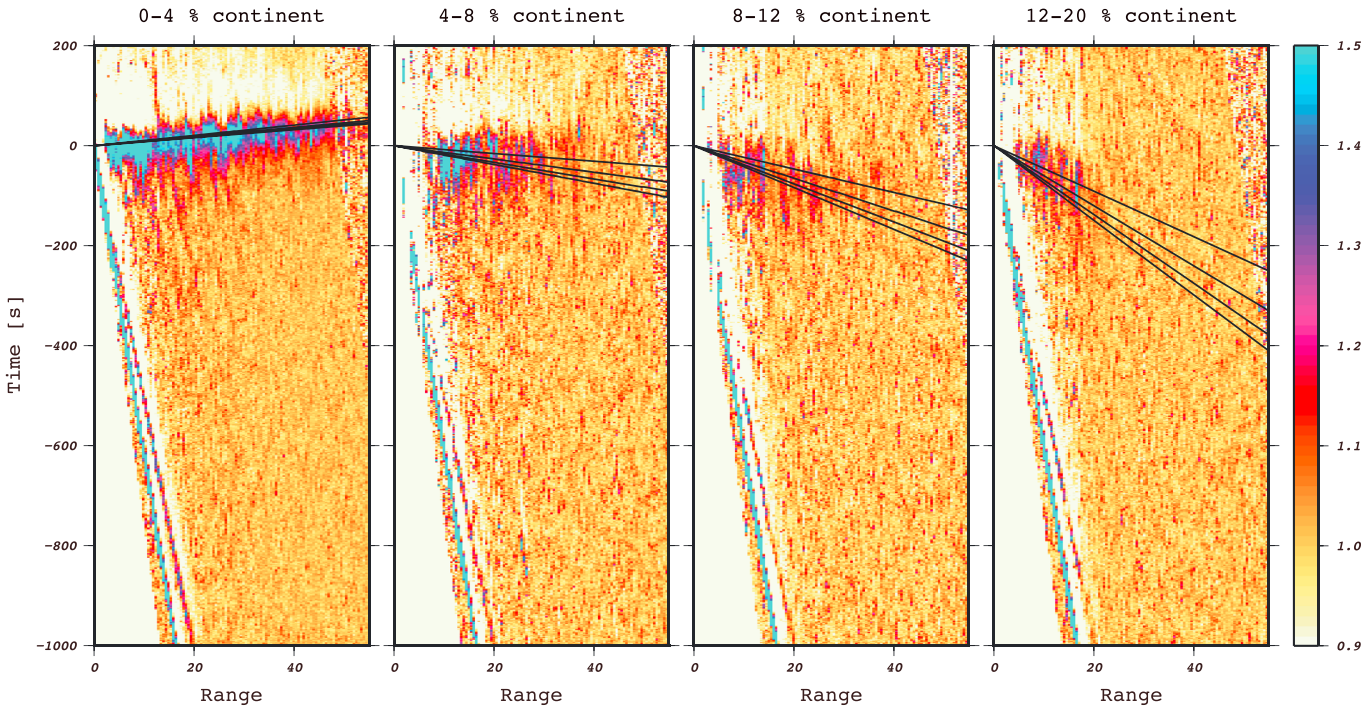

Figure 5. Stacks with subset of data from *T* phase paths with different percentage of continental path length. Black lines correspond to crustal velocity 3–6 km/s and an apparent *T* phase velocity of 1.47 km/s.

continental distance. Figure 5 shows how an increase in percentage of the continental path changes the slope of the *T* phase arrival (the stack is produced with a reduction velocity of 1.5 km/s). For 0–4% continental path length, the *T* phase appears to propagate with an apparent velocity below 1.5 km/s, and arrival times computed with 1.47 km/s fit the energy in the stacks the best. The *T* phase becomes less visible for longer continental paths, and the stacks suggest that there is not much energy contributing from receivers more than 4° away from the coast. The resolution of the stacks is currently not good enough to resolve average crustal *P* velocities or distinguish between different converted phases (the STA/LTA filtering and the characteristic long wave train of the *T* phase composed of probably both Pg and Sg energy *Cansi and Bethoux* [1985] and *Stevens et al.* [2001] make this challenging), but the slopes and offset times agree with reasonable crustal velocities between 3 and 6 km/s.

4. Summary

We show that the T-phase can be clearly observed in stacks of STA/LTA filtered seismograms from land seismometers of the GSN. The signal is most visible at frequencies above 2 Hz. It is important to be aware of coherent energy late in seismograms, as this might influence surface-wave studies or noise assessments. The resolution of the stacks is not good enough to obtain detailed information on average crustal velocities, but observed changes in the stacks for different subsets of data agree with the theory of acoustic to seismic coupling of the energy at continents. Including more stations, such as USArray or the stations in Japan [*Kosuga*, 2011] could potentially increase resolution. In addition, more data could permit stacking for specific locations/paths in order to analyze regions of T-phase blockage in more detail. This could be useful for explosion monitoring [*Harben et al.*, 2002].

Acknowledgments
All data are available from the IRIS DMC.

The Editor thanks two anonymous reviewers for their assistance in evaluating this paper.

References

Astiz, L., P. Earle, and P. Shearer (1996), Global stacking of broadband seismograms, *Seismol. Res. Lett.*, *67*(4), 8–18, doi:10.1785/gssrl.67.4.8.

Buehler, J., and P. Shearer (2013), Sn propagation in the Western United States from common midpoint stacks of USArray data, *Geophys. Res. Lett.*, *40*, 6106–6111, doi:10.1002/2013GL057680.

Cansi, Y., and N. Bethoux (1985), T waves with long inland paths: Synthetic seismograms, *J. Geophys. Res.*, *90*(B7), 5459–5465.

Chapman, N. R., and R. Marrett (2006), The directionality of acoustic T-phase signals from small magnitude submarine earthquakes, *J. Acoust. Soc. Am.*, *119*(6), 3669–3675, doi:10.1121/1.2195073.

de Groot-Hedlin, C. D., and J. A. Orcutt (1999), Synthesis of earthquake-generated T-waves, *Geophys. Res. Lett.*, *26*(9), 1227–1230, doi:10.1029/1999GL900205.

de Groot-Hedlin, C., and J. Orcutt (2001), T-phase observations in Northern California: Acoustic to seismic coupling at a weakly elastic boundary, *Pure Appl. Geophys.*, *158*(3), 513–530.

Earle, P. S., and P. M. Shearer (1994), Characterization of global seismograms using an automatic-picking algorithm, *Bull. Seismol. Soc. Am.*, *84*(2), 366–376.

Harben, P. E., C. de Groot-Hedlin, and D. Blackman (2002), Acoustic sources for blockage calibration of ocean basins: Results from the October 2001 Indian Ocean cruise, paper presented at 24th Seismic Research Review, Nuclear Explosion Monitoring: Innovation and Integration, Ponte Vedra Beach, Fla., 17–19 Sept.

Johnson, R. H., J. Northrop, and R. Eppley (1963), Sources of Pacific T phases, *J. Geophys. Res.*, *68*(14), 4251–4260.

Kosuga, M. (2011), Localization of T-wave energy on land revealed by a dense seismic network in Japan, *Geophys. J. Int.*, *187*(1), 338–354.

Okal, E. A. (2008), *The Generation of T Waves by Earthquakes*, pp. 1–65, Elsevier, London.

Richards-Dinger, K. B., and P. M. Shearer (1997), Estimating crustal thickness in southern California by stacking PmP arrivals, *J. Geophys. Res.*, *102*(B7), 15,211–15,224.

Rodgers, A., and P. Harben (2000), T-Phase observations from the May 1999 Ascension Island experiment, Tech. Rep., Lawrence Livermore National Laboratory, Livermore, CA, 94550, Proceedings of the 22nd Annual DoD/DOE Seismic Research Symposium: Planning for Verification of and Compliance with the Comprehensive Nuclear-Test-Ban Treaty (CTBT) held in New Orleans, U.S. Government or Federal Rights, Louisiana, 13–15 Sept.

Stevens, J., G. Baker, R. Cook, G. D'Spain, L. Berger, and S. Day (2001), Empirical and numerical modeling of T-phase propagation from ocean to land, *Pure Appl. Geophys.*, *158*(3), 531–565.

Talandier, J., and E. A. Okal (1998), On the mechanism of conversion of seismic waves to and from t waves in the vicinity of island shores, *Bull. Seismol. Soc. Am.*, *88*(2), 621–632.

Walker, D. A., C. S. McCreery, and Y. Hiyoshi (1992a), T-phase spectra, seismic moments, and tsunamigenesis, *Bull. Seismol. Soc. Am.*, *82*(3), 1275–1305.

Walker, D. A., C. S. McCreery, and Y. Hiyoshi (1992b), T-phase spectra, seismic moments, and tsunamigenesis, *Bull. Seismol. Soc. Am.*, *82*(3), 1275–1305.